JOURNAL OF GEOPHYSICAL RESEARCH, VOL. 108, NO. D18, 4571, doi:10.1029/2002JD003331, 2003

Column-integrated aerosol optical properties from ground-based spectroradiometer measurements at Barrax (Spain) during the Digital Airborne Imaging Spectrometer Experiment (DAISEX) campaigns

Roberto Pedrós, Jose A. Martinez-Lozano, Maria P. Utrillas, José L. Gómez-Amo, and Fernando Tena

Grupo de Radiación Solar, Departamento de Termodinámica, Universitat de Valencia, Valencia, Spain

Received 19 December 2002; revised 29 May 2003; accepted 11 June 2003; published 17 September 2003.

[1] The Digital Airborne Imaging Spectrometer Experiment (DAISEX) was carried out for the European Space Agency (ESA) in order to develop the potential of spaceborne imaging spectroscopy for a range of different scientific applications. DAISEX involved simultaneous data acquisitions using different airborne imaging spectrometers over test sites in southeast Spain (Barrax) and the Upper Rhine valley (Colmar, France, and Hartheim, Germany). This paper presents the results corresponding to the column-integrated aerosol optical properties from ground-based spectroradiometer measurements over the Barrax area during the DAISEX campaign days in the years 1998, 1999, and 2000. The instruments used for spectral irradiance measurements were two Licor 1800 and one Optronic OL-754 spectroradiometers. The analysis of the spectral aerosol optical depth in the visible range shows in all cases the predominance of the coarse-particle mode over the fine-particle mode. The analysis of the back trajectories of the air masses indicates a predominance of marine-type aerosols in the lower atmospheric layers in all cases. Overall, the results obtained show that during the DAISEX there was a combination of maritime aerosols with smaller continental aerosols. *INDEX TERMS:* 0305 Atmospheric Composition and Structure: Aerosols and particles (0345, 4801); 0345 Atmospheric Composition and Structure: Pollution—urban and regional (0305); 0394 Atmospheric Composition and Structure: Instruments and techniques; 3360 Meteorology and Atmospheric Dynamics: Remote sensing; 4801 Oceanography: Biological and Chemical: Aerosols (0305); *KEYWORDS:* atmospheric composition and structure, instruments and techniques, remote sensing

Citation: Pedrós, R., J. A. Martinez-Lozano, M. P. Utrillas, J. L. Gómez-Amo, and F. Tena, Column-integrated aerosol optical properties from ground-based spectroradiometer measurements at Barrax (Spain) during the Digital Airborne Imaging Spectrometer Experiment (DAISEX) campaigns, *J. Geophys. Res.*, *108*(D18), 4571, doi:10.1029/2002JD003331, 2003.

1. Introduction

[2] Since the mid-1980s the European Space Agency (ESA) has carried out airborne campaigns and other studies aimed at developing the potential of spaceborne imaging spectroscopy for a range of different scientific applications. The latest of these activities, the Digital Airborne Imaging Spectrometer Experiment (DAISEX), involved simultaneous data acquisitions using three different airborne imaging spectrometers over test sites in southeast Spain (Barrax) and the Upper Rhine valley (Colmar, France, and Hartheim, Germany) [*ESA*, 2001a]. Results from DAISEX provide important contributions toward preparations for satellite missions such as the Medium Resolution Imaging Spectrometer (MERIS) that was recently launched on Envisat. Looking to the future Earth Explorer missions [*ESA*, 2001b], the interest of results from DAISEX field campaigns are centered on the Surface Processes and Ecosystems Changes Through Response Analysis (SPECTRA) mission.

[3] The main scientific objectives of DAISEX were to demonstrate the retrieval of geo/biophysical variables from imaging spectrometer data. Target variables included surface temperature, leaf area index, canopy biomass, leaf water content, canopy height, canopy structure, and soil properties [*Berger et al.*, 2001]. Accurate calibration and atmospheric correction of imaging spectrometer data are vital for retrieving such variables, and the DAISEX campaigns included both atmospheric measurements, needed for atmospheric correction, and ground spectroradiometer measurements to validate the calibrated data.

[4] Atmospheric aerosols are currently the principal cause of uncertainty in atmospheric correction models. Season and location are only partial predictors of aerosol optical properties, while aerosol size, for instance, can vary significantly from day-to-day at a single location [*Holben et al.*, 1996; *Remer and Kaufman*, 1998]. Such day to day variations stem from meteorological variability rather than direct changes in the strength of aerosol sources. Aerosol optical properties are particularly dependent on the air mass resi-

0148-0227/03/2002JD003331$09.00

dence times and the duration of stagnant conditions [*Remer et al.*, 1999]. More information (and more detailed) is needed on the atmospheric aerosols' optical and radiative properties and their distribution in space and time [*Schwartz and Andreae*, 1996; *Penner et al.*, 2001]. Algorithms need to be developed that can relate these properties to those parameters that are most easily measured from satellites. Data are given in the special issue "Passive remote sensing of the tropospheric aerosol and atmospheric corrections of the aerosol effect" in *Journal of Geophysical Research*, *102*, 1997.

[5] One of the most reliable means of determining the optical and physical properties of the total aerosol column is the combination of two methods: airborne in situ measurements and ground-based remote sensing [*Remer et al.*, 1997]. In the DAISEX campaigns (a detailed description of which is presented in the following section) simultaneous measurements of this type were available for 2 days of the DAISEX-99 campaign, from a lidar and a nephelometer on board the airborne Avion de Recherche Atmosphérique et de Télédéction (ARAT). Some results related to these have been published by the authors in a previous paper [*Martínez-Lozano et al.*, 2002]. In this paper we present the results corresponding to the column-integrated aerosol optical properties over the Barrax area during all the days of the DAISEX campaign. We have started from the determination of the Aerosol Optical Depth (hereafter AOD) from solar irradiance extinction measurements at ground level (a.g.l.). The AOD is the single most comprehensive variable to remotely assess the aerosol burden in the atmosphere from ground-based instruments, which are the simplest, most accurate, and easy to maintain monitoring systems [*Holben et al.*, 2001].

2. Measurement Campaigns

[6] The DAISEX campaigns in Spain were carried out in the area of La Mancha, a plateau located 700 m above sea level (see Figure 1). The area was originally selected due to its flat morphology and the presence of large, uniform land-use units, suitable for validation of moderate-resolution satellite instruments. The main activities in this area started when the area was selected as test site for the European International Project on Climatic and Hydrological Interactions between Vegetation, Atmosphere and Land Surface, Field Experiment in Desertification Threatened Areas (European International Project on Climatic and Hydrological Interactions (EFEDA)) experiment in 1991 [*Bolle et al.*, 1993]. The Barrax area was also selected by ESA as a test site for the preparation activities for the Land Surface Processes and Interactions Mission (LSPIM), as well as SPECTRA, which are two Earth Explorer Candidate Core Missions [*ESA*, 1999, 2001b]. The DAISEX campaigns were carried out as a part of these activities [*Berger et al.*, 2000, 2001]. The climatic and geomorphological properties of the Barrax area, as well as the permanent facilities for surface fluxes and meteorological data, have been previously described by *Moreno et al.* [2001].

[7] The DAISEX campaigns at Barrax took place during the summers of 1998, 1999, and 2000. The DAISEX-98 campaign was a single-day campaign in August, limited to providing images of the Digital Airborne Imager Spectrometer (DAIS) sensor [*Chang et al.*, 1993] operated by the German Aerospace Agency on board the DLR/Dornier aircraft. The DAISEX-99 campaign was the main campaign in the whole DAISEX activity and was clearly the core of the DAISEX activities in Barrax. It took place in June 1999. As well as DAIS, another hyperspectral sensor was available, Hyperspectral Mapping (HYMAP) [*Cocks et al.*, 1998]. The two sensors, DAIS and HYMAP, were flown together on board the DLR/Dornier aircraft. In addition to the DLR/Do228, a second airborne platform, the multiagency INSU/CNES/IGN/Météo-France ARAT, accessible within the framework of the Scientific Training and Access to Aircraft for Atmospheric Research Throughout Europe (STAAARTE) Program, also participated in DAISEX-99. Both the backscatter Lidar embarqué pour l'Eude des Aerosols et des Nuages, de l'interaction Dynamique-Rayonnement et du cycle de l'Eau (LEANDRE) aerosol lidar [*Flamant and Pelon*, 1996] and the POLDER multiangular imaging sensor [*Deschamps et al.*, 1994] operated simultaneously on board the ARAT aircraft. The DAISEX-2000 campaign (DAISEX-99 extension) was similar in scope to the DAISEX-98 campaign as it was a single-day campaign. Two aircrafts were available in this case, one carrying the DAIS and Reflective Optics System Imaging Spectrometer (ROSIS) [*Gege and Mooshuber*, 1997] sensors, and another carrying the HYMAP sensor.

Figure 1. Location of the Barrax study area selected for the DAISEX campaigns.

[8] Apart from the permanent experimental facilities located in the Barrax area [*Moreno et al.*, 2001], many additional instruments were deployed in the field to take additional measurements specifically for the DAISEX campaigns. The Solar Radiation Group of Valencia University actively participated in the three DAISEX campaigns in Barrax in order to obtain ground-level solar spectral irradiance and sky radiance data in the visible range. The spectral irradiance and radiance measurements were made using two Licor 1800 and one Optronic OL-754 spectroradiometers. Spectroradiometric measurements were made at the same location for all three campaigns, beside the Lysimetric station at Las Tiesas (Barrax), during the days 11 August 1998; 3, 4, and 5 June 1999; and 29 June 2000. A detailed description of these can be found in the work by *Utrillas et al.* [2001]. The measurement of solar irradiance with high spectral resolution (<0.01 μm) permits (1) separation of the aerosol signal from that produced by molecular scattering

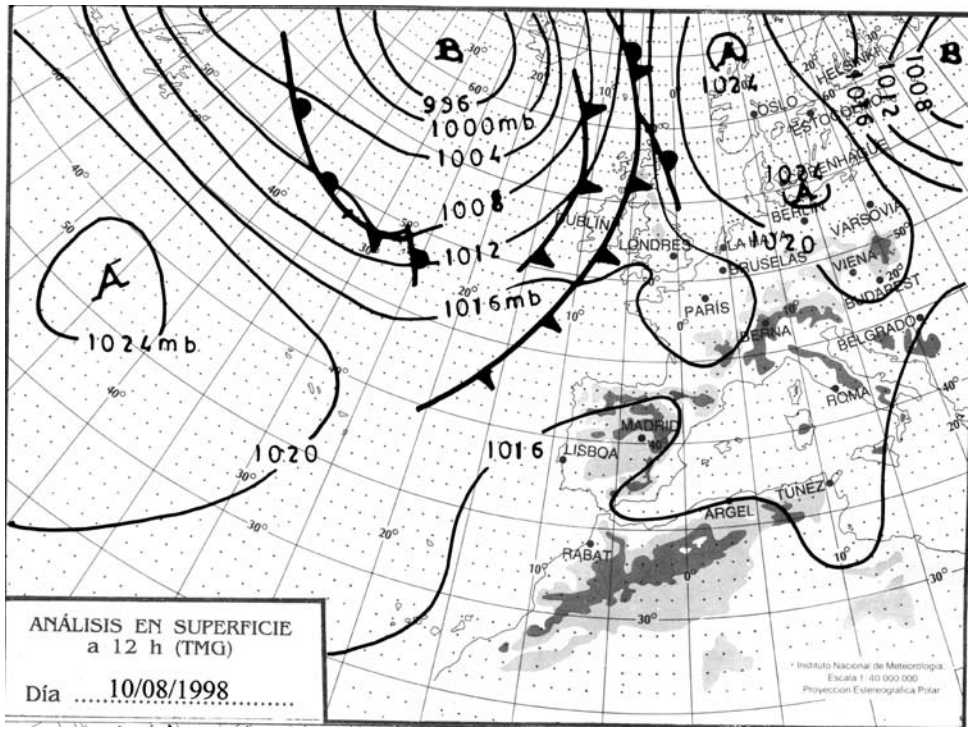

Figure 2. Surface isobaric map for the DAISEX-98 campaign.

and absorption, (2) retrieval of aerosol optical parameters, and (3) estimation of the aerosol microphysical characteristics, such as the aerosol size distribution [*Vasilyev et al.*, 1995]. The subsequent processing of these data has allowed, for instance, the atmospheric correction of the POLDER images [see, for example, *Ponchaut*, 2000].

[9] The Licor 1800 is a single monochromator spectroradiometer in the 300–1100 nm range. The optical receptor is a PTFE (Teflon) dome with a 2π steradian Field of View (FOV). The monochromator is a motor-driven scanning-type holographic grating with a 6-nm Full-Width at Half-Maximum (FWHM) and a band-pass precision of 1 nm. The detector is a silicon photodiode operating in the photovoltaic mode. For the measurement of the direct component a radiance-limiting tube (collimator) with a FOV of 4.6° and a system of alignment was coupled to the Teflon diffuser of the receptor, and the spectroradiometer was oriented manually on a tripod with the help of a three-axis joint.

[10] The Optronic OL-754 is a high-precision double monochromator spectroradiometer in the 250–800 nm range with a photomultiplier as sensor element. The double monochromator has two concave holographic grids with 1200 grooves/mm, the FWHM is 1.6 nm, and the band-pass precision is 0.05 nm. For measuring the global irradiance the aperture of the optical head is connected to an integrating sphere with a hemispherical dome of fused quartzite attached over the entrance slit. For the direct irradiance measurements a collimator is used to limit the FOV to 5.72°. For measurements of the direct solar irradiance the spectroradiometer is mounted on a tripod with a fixture that permits movement in three directions, similar to that used by the Licor 1800. The mobility of the integrating sphere, which permits the entrance point of the optical head to be rotated through 360°, could also be used.

[11] The authors have analyzed the uncertainties associated with these spectroradiometers in the visible range [*Martínez-Lozano et al.*, 2003]. The overall uncertainty (root square sum of the uncertainties) is ±5.0% for the Licor 1800 and ±3.7% for the Optronic 754. These values include both the uncertainties related to the calibration and those related to the measurement process; however, if only the uncertainties associated with the measurement process are considered then the values are ±4.4% for the Licor 1800 and ±2.7% for the Optronic 754. When both instruments were compared in the visible range the deviations were less than 2% [*Martínez-Lozano et al.*, 2003].

3. Meteorology

[12] Figures 2–4 show surface isobaric maps produced by the Spanish Meteorological Institute using High-Resolution Limited Area Model (HIRLAM) in collaboration with the European Centre for Medium range Weather Forecasts (ECMWF) (see http://hirlam.knmi.nl/). During the DAISEX-98 campaign (Figure 2) the surface map shows that the situation over the Iberian Peninsula was predominantly a thermal low, with a low-pressure gradient, that also appears reflected in the 850-hPa isotherm field. In the middle and higher layers of the troposphere the situation is predominantly a weak flow from the west. For the DAISEX-2000 campaign (Figure 4) a low-pressure area can also be seen a.g.l. over the eastern peninsula, with a warm ridge at 850 hPa affecting the area of Castilla La Mancha (measurement zone). At 500 hPa there is a ridge with its axis over the center of the Iberian Peninsula and a flow with a predominantly western component.

[13] During the DAISEX-99 campaign (Figure 3) the synoptic situation is different. Initially, it is governed by

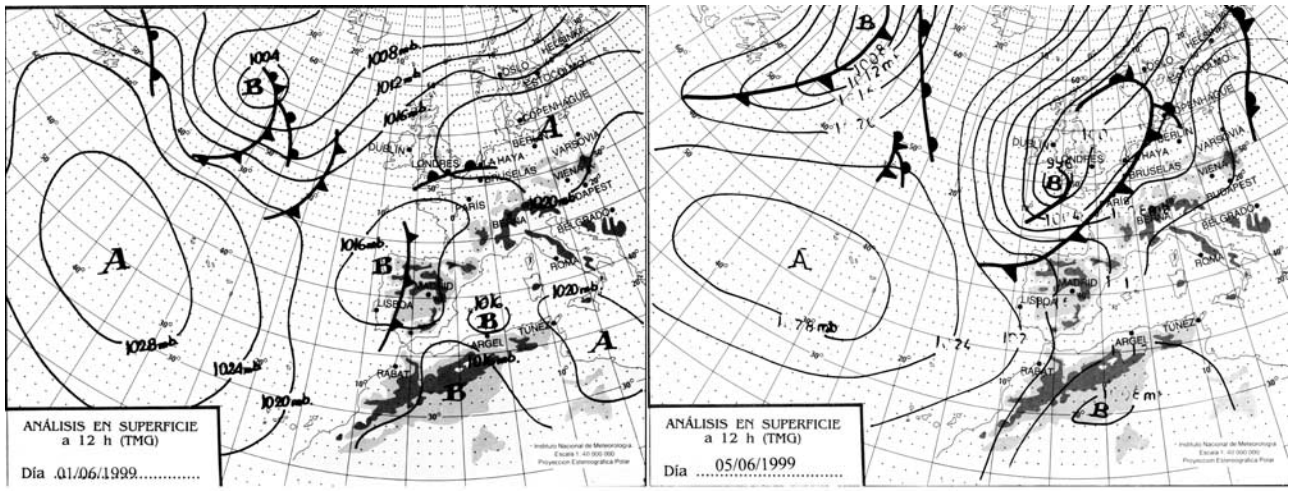

Figure 3. Surface isobaric maps for the DAISEX-99 campaign. (a) 1 June 1999; (b) 5 June 1999.

the passing of a cold front, which is found at 1200 UTC on day 1, located over the western third of the Iberian Peninsula (Figure 3a), and at 1200 UTC on day 2, located in the Mediterranean over the Balearic Islands, passing over Barrax during the night of 1–2 June. In the 850-hPa isotherm this front is clearly seen, together with the change of air mass produced by its passing. At 500 hPa the most noticeable element on day 1 is the presence of a low front over the Portuguese coast inducing an intense general airflow from the SW over the Iberian Peninsula, while on day 2 a trough is appreciable along the length of the axis of the Bay of Biscay-Bay of Valencia, with a predominant W-SW flow over the measurement area, giving rise to moderate intensity rainfall. On the measurement days, days 3–5 of June, the surface situation remained stable, with a predominance of high pressures over the Peninsula with low barometric gradient. Simultaneously, in the medium-high layers predominated a weak flow from the west over the measurement area. This situation tended to disappear toward the end of the period (Figure 3b), with the Peninsula beginning to come under the influence of a cyclone situated over the British Isles.

[14] Aerosol optical properties are strongly dependent on the evolution of synoptic air masses and associated regions and to a certain extent can be uniquely characterized by the air mass type and source [*Smirnov et al.*, 1995, 2000; *Moorthy et al.*, 2003]. It is also necessary to remember that the analysis from measurements of spectral direct solar

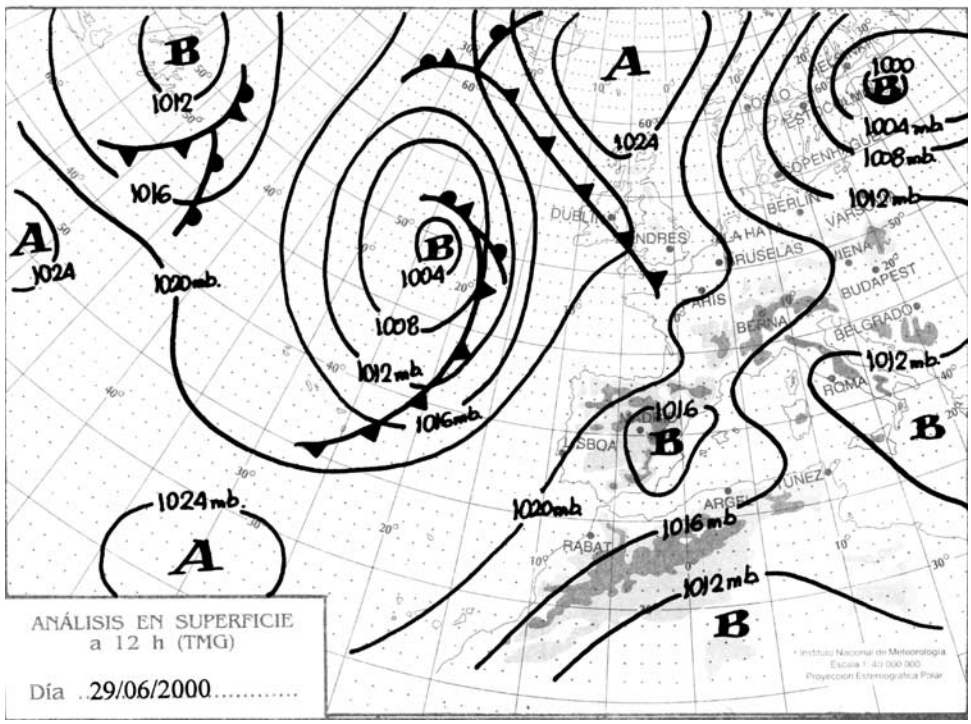

Figure 4. Surface isobaric map for the DAISEX-2000 campaign.

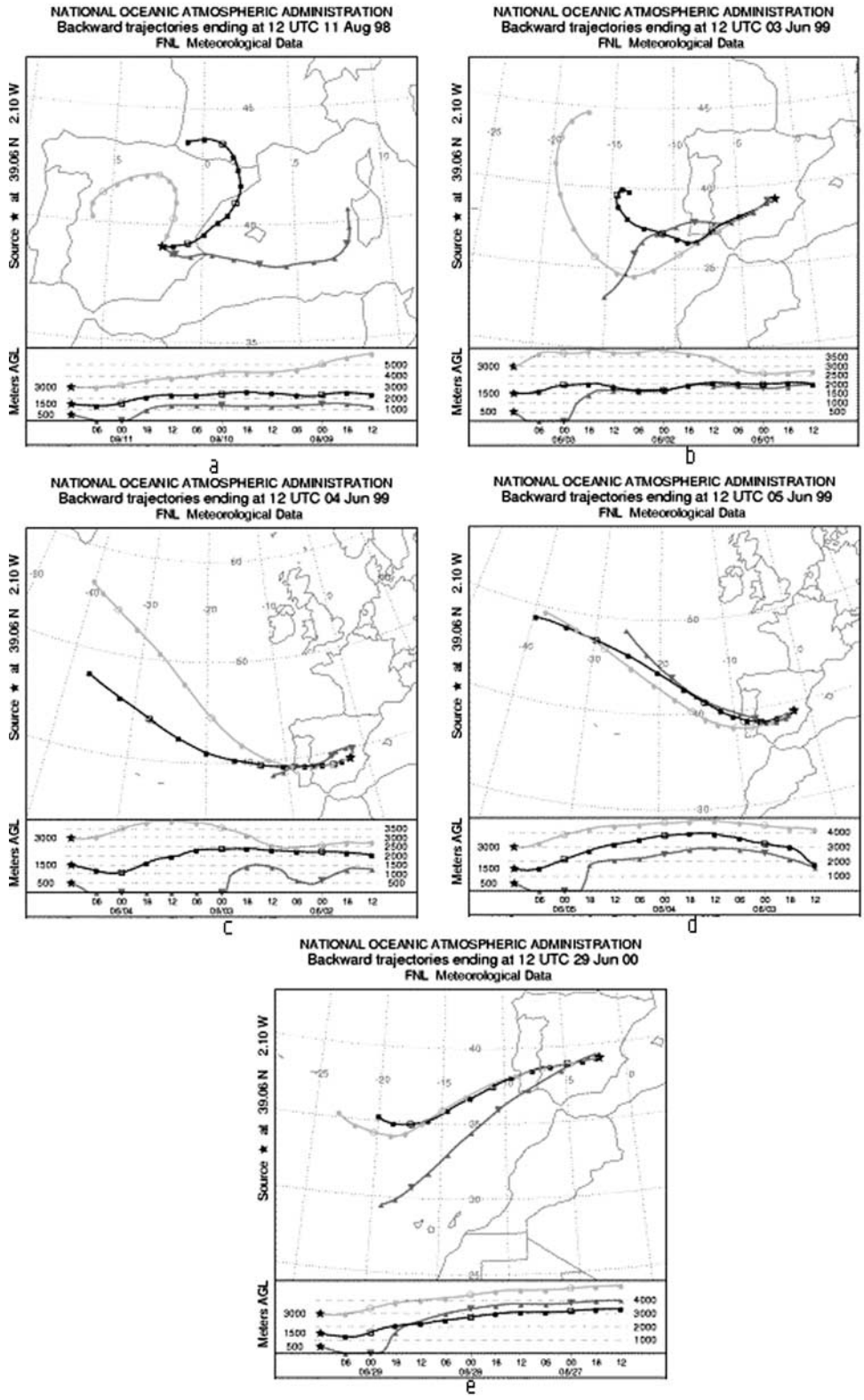

Figure 5. Three-day back trajectories computed with HYSPLIT4 ending at 1200 UTC in Barrax: (a) 11 August 1998; (b) 3 June 1999; (c) 4 June 1999; (d) 5 June 1999; and (e) 29 June 2000.

irradiance is representative of the aerosol optical properties integrated over the entire atmospheric column from the surface to the top of the atmosphere. Therefore the derived parameters are the radiatively effective column-integrated values that can be composed of a set of values from distinct layers, which contain aerosols that may originate from different source region [*Eck et al.*, 2001a]. It is therefore necessary to consider the air masses at different altitudes.

[15] Three-day back trajectories computed with the Hybrid Single-Particle Lagrangian Integrated Trajectory

(HYSPLIT4) Model (see http://www.noaa.gov/ready/hysplit4.htmel), ending at 1200 UTC in Barrax, were used to characterize the origin of the air masses arriving over the measurement site at 500, 1500, and 3000 m above ground level. Figures 5a–5e show these back trajectories for the days of the campaigns. Trajectory analyses for Barrax showed similar air mass source regions for both 1999 and 2000, with an Atlantic origin in the different altitudes considered, which agrees with the surface maps described above. The trajectories for 1998, Figure 5a, showed a combination of air masses of Mediterranean maritime origin a.g.l., together with Atlantic origin air masses at 1500 and 3000 m a.g.l., which are found during most of their trajectory above the Iberian Peninsula. Wind direction data a.g.l. acquired from meteorological station in the study area [*Gonzalez et al.*, 2001] agree with the back trajectories at 500 m a.g.l.

[16] During the three measurement campaigns two kinds of atmospheric measurements were made simultaneously to the flights: (1) free soundings launched by the Spanish National Institute of Meteorology and (2) total precipitable water content and total column ozone content. The results of these measurements are given by *Gonzalez et al.* [2001]. We give here only a summary of the most relevant results. During the DAISEX 1998 campaign the AS-1C-PTH radiosondes model was used. These radiosondes measure bulb temperature, dry temperature, and pressure. Figure 6 shows the vertical temperature and relative humidity profiles for this campaign. For the DAISEX 1999 and 2000 campaign the RS80 ozonesondes manufactured by the Vaisala company were used. The RS80 Vaisala sonde is composed of absolute pressure, temperature, and humidity sensors and an electrochemical concentration cell ozone sensor. In Figures 7a–7c and 8 the vertical profiles of temperature and relative humidity are shown for these two campaigns. For the DAISEX-98 and DAISEX-00 campaign days the vertical profiles of temperature show indifferent or fair stability, as is corroborated by the relative humidity profiles which are practically constant in the first kilometers from the ground. The days of the DAISEX-99 campaign show higher stability with temperature profiles showing inversion zones at different heights depending on the day. These results are consistent with those obtained from the relative humidity profiles, in which maximum values are observed at heights corresponding to the inversion layer for each of the temperature profiles. Table 1, taken from the work of *Gonzalez et al.* [2001], shows a summary of all the sondes launched over the different campaigns. In situ ozone measurements were not possible for the 1998 campaign. However, the National Institute of Meteorology provided a column-integrated ozone value of 306.0 Dobson units (DU) measured in Madrid around noon on 11 August. It can be considered that the ozone measured in Madrid (200 km from Barrax) is still representative of the conditions in Barrax as the altitude over the sea is more or less the same in both places and the meteorological conditions were very similar.

[17] Column water and ozone atmospheric content have also been measured using a Microtops II sunphotometer. Tables 2 and 3 compare the corresponding values of water and ozone columnar content, respectively, obtained from the atmospheric sondes and the Microtops II sunphotometer.

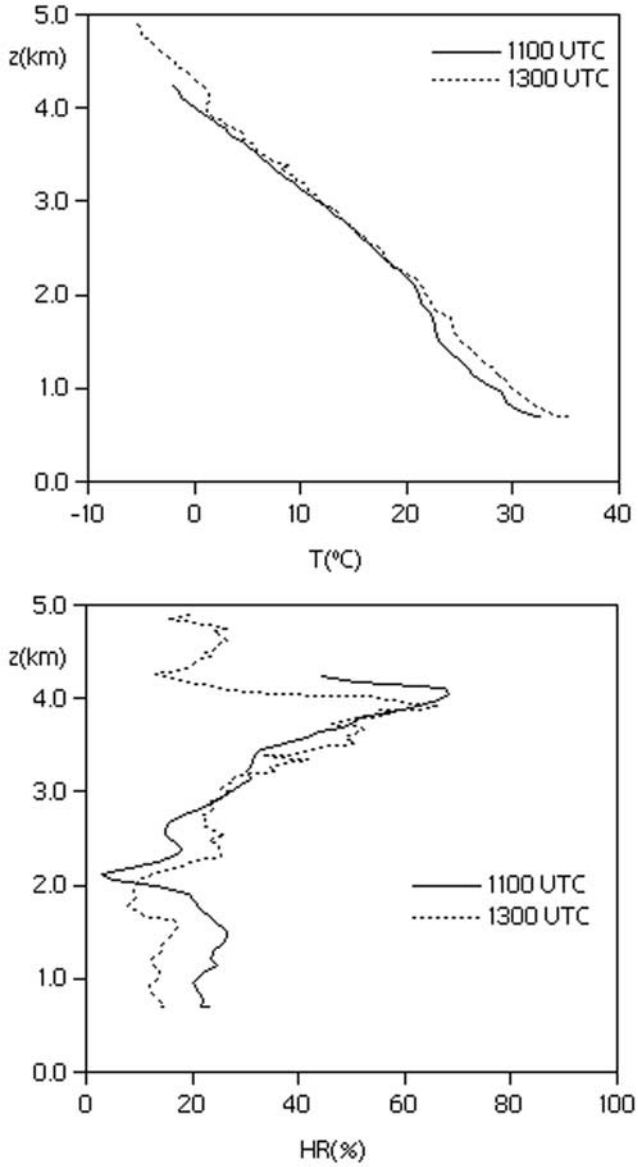

Figure 6. Vertical temperature and relative humidity profiles for the DAISEX-98 campaign.

Ozone soundings typically reach altitudes of 30 km, which is the altitude where the maximum concentration of atmospheric ozone is located. This fact makes it necessary to complete the measured profile. In all cases, the profiles have been completed until 100 km with the most similar standard atmosphere, in this case midlatitude summer.

[18] From Tables 2 and 3 it is possible to analyze the utility of the Microtops II sunphotometer for determining column values of both ozone and water vapor in the absence of sondes. It can be seen that the deviations present in the ozone measurements (Table 3) stay at acceptable levels, in no case reaching above 10%. However, the water vapor measurements (Table 2) show deviations that make them invalid, indicating the need to perform a recalibration of the channel filter in order to determine water vapor with our instrument. Nevertheless, it should be noted that for determining spectral AOD in the visible range, the purpose of

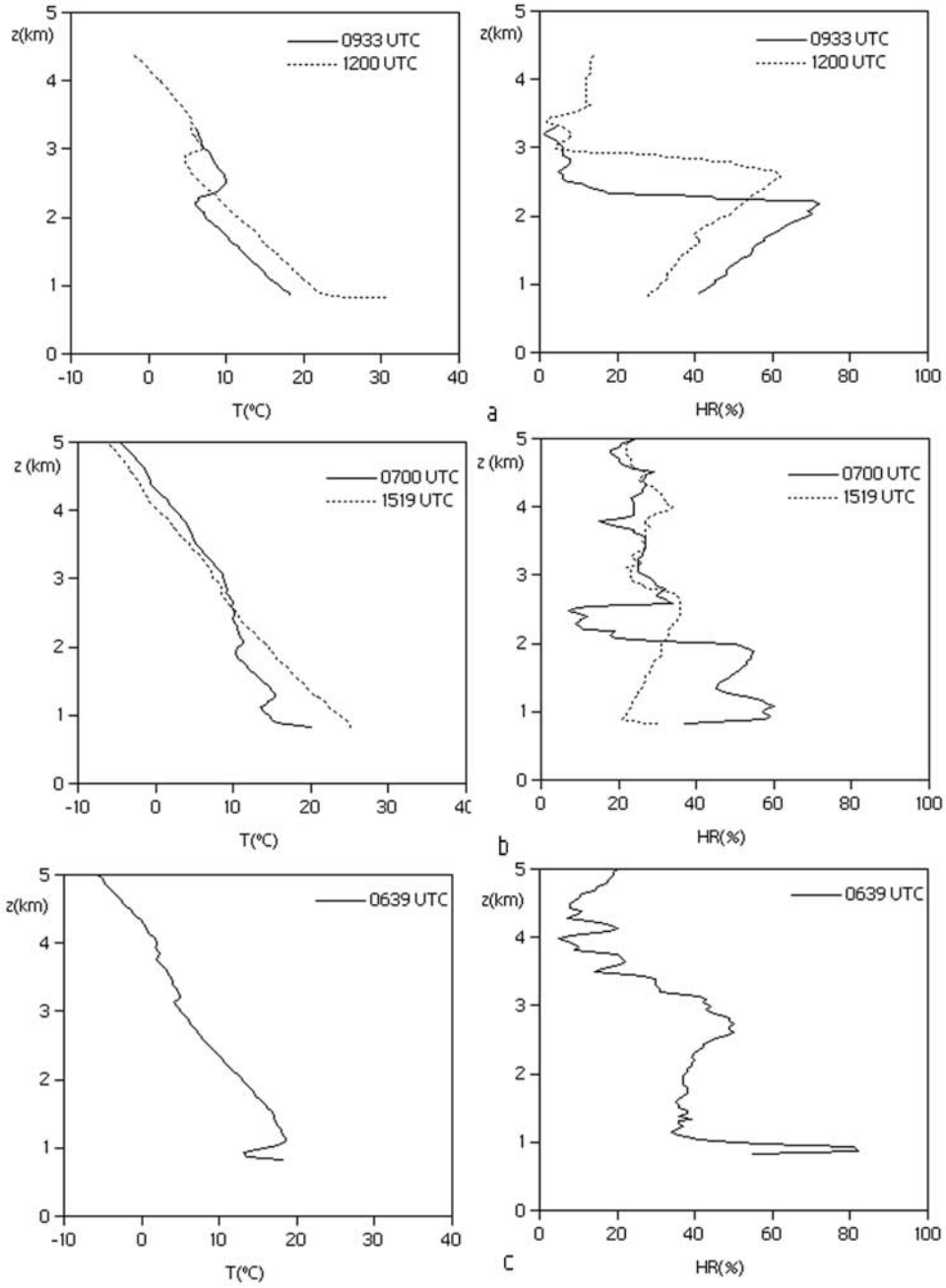

Figure 7. Vertical temperature and relative humidity profiles for the DAISEX-99 campaign: (a) 3 June 1999; (b) 4 June 1999; and (c) 5 June 1999.

this work, the water vapor content values are not needed. For the correction for ozone, which must be done in the Chappuis band, as explained in detail in the following section, in every case the values provided by ozone sondes were used.

4. Methodology

[19] The total atmospheric optical depth, $\tau_{T\lambda}$, is determined from the spectral irradiance measurements at normal incidence using the Bouger-Lambert-Beer exponential law. This total optical depth can be expressed, in the visible range, as the sum of the optical depths related to the different atmospheric components:

$$\tau_{T\lambda} = \tau_{R\lambda} + \tau_{a\lambda} + \tau_{O\lambda} + \tau_{w\lambda} + \tau_{N\lambda}, \quad (1)$$

where $\tau_{R\lambda}$ is the molecular scattering optical depth (which is usually calculated using the Rayleigh approximation), $\tau_{a\lambda}$ is the aerosol extinction optical depth, and $\tau_{O\lambda}$, $\tau_{w\lambda}$, and $\tau_{N\lambda}$ are the optical depths due to O_3, H_2O, and NO_2 absorption, respectively.

[20] Once the total atmospheric optical depth is determined, values of $\tau_{a\lambda}$ can be obtained by eliminating

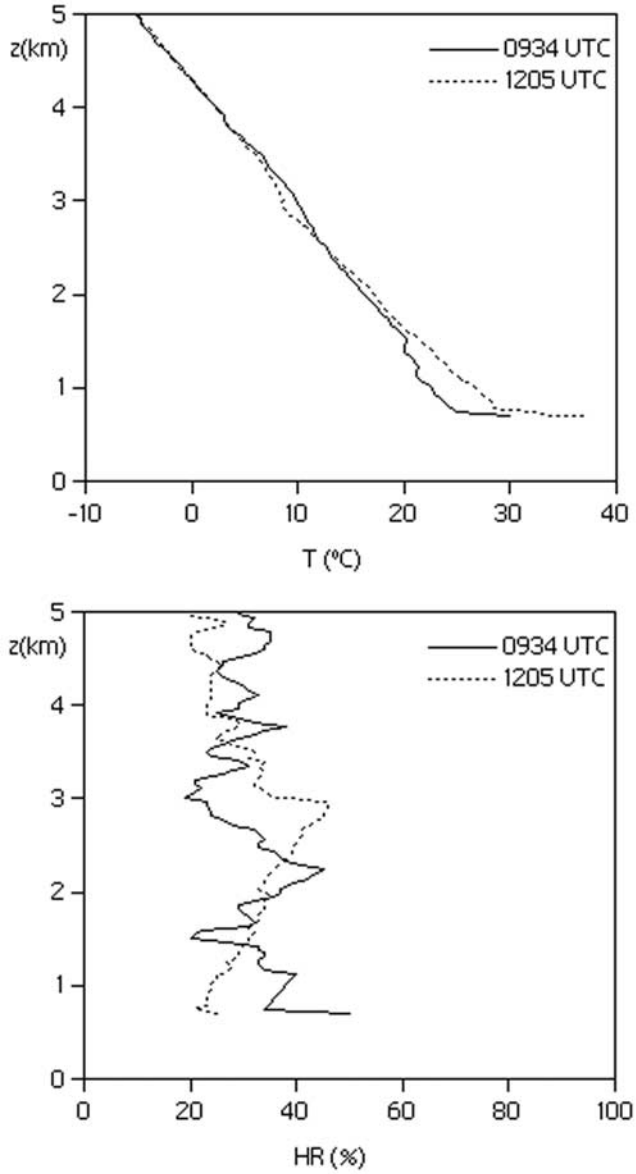

Figure 8. Vertical temperature and relative humidity profiles for the DAISEX-2000 campaign.

contributions due to Rayleigh scattering and to absorption by other atmospheric components from the total transmittance. In this case, although our spectral irradiance measurements ranged from 300 to 1100 nm, we limited the study of the spectral AOD to the 400–670 nm band, where the only components showing nonnegligible absorption are ozone (Chappuis band) and NO_2. In this way the errors introduced by all the other atmospheric constituents in the parameterization of the AOD are eliminated. The absorption due to NO_2 has not been considered due to the rural character of the measurement site. However, the correction due to ozone is necessary since the optical depth of ozone in the Chappuis band represents, on average, 8% of the total atmospheric optical depth. This value depends on the wavelength, being only 4% at 500 nm.

[21] To determine $\tau_{T\lambda}$, we employed the values of the extraterrestrial spectrum proposed by the SMARTS2 model [*Gueymard*, 2001], smoothing the data to the band pass of

Table 1. Summary of the DAISEX Campaigns Soundings

YMD[a]	Starting Time, UTC	Duration, min	Final Altitude,[b] gpm
	DAISEX-98		
980811	1104	12	4241
	1300	15	4908
	DAISEX-99		
990603	0933	9	3299
	1204	14	4397
990604	0705	104	31,743
	1519	101	31,955
990605	0639	103	22,488
	DAISEX-00		
000629	0934	102	32,278
	1205	92	30,189

[a]YMD, year, month, day; read 980811 as 11 August 1998.
[b]Gpm, geopotential height, meters.

our spectroradiometer. For the air mass, the empirical expression proposed by *Kasten and Young* [1989] was used. The Rayleigh optical depth was calculated from the approximation by *Bodhaine et al.* [1999]. The ozone absorption coefficients by *Anderson and Mauersberger* [1992] were assumed, and the total ozone amount was retrieved from the ozone soundings performed by the Spanish National Meteorological Institute.

[22] Error propagation methods were applied to obtain the AOD error. *Utrillas* [1995] developed a simplified method to estimate the error associated with the AOD values retrieved from spectral irradiance measurements. This method is similar to that developed by *Russell et al.* [1993] and *Schmid et al.* [1997]. In our case the error in the AOD is mainly conditioned by the error in the measurement of the direct spectral irradiance and the value of the optical mass in the instant of the measurement, presenting maximum values when the optical mass values are one. The authors have previously used this method with experimental measurements made at other sites [*Martínez-Lozano et al.*, 2001; *Estellés et al.*, 2003], and the values that were obtained were similar to those presented by *Kaufman et al.* [1994]. The authors have also estimated, using the Nakajima SKYRAD.PACK code [*Nakajima et al.*, 1983, 1996], the contribution of the sky radiance to the measured irradiance, due to the fact that the solid angle subtended by the collimators is higher than the solid angle subtended by the sun. The inaccuracy due to the circumsolar radiation, for 500 nm, was 0.6% assuming that the sun was perfectly centered in the instrument's FOV [*Martínez-Lozano et al.*, 2002, 2003]. When the Sun was not in the center, the

Table 2. Columnar Water Vapor From Atmospheric Soundings and From Sunphotometer Microtops II

YMDH[a]	Sounding, g/cm^2	Microtops II, g/cm^2
9808111100	1.55	not available
9808111300	1.35	not available
9906030933	1.21	0.57
9906031204	1.09	0.57
9906040705	1.35	0.79
9906041519	1.24	0.79
9906050639	1.35	0.79
0006290934	1.59	0.90
0006291205	1.59	0.90

[a]YMDH, year, month, day, hour; read 9808111100 as 11 August 1998, 1100 UT.

Table 3. Columnar Ozone Column From Atmospheric Soundings and From Sunphotometer Microtops II

YMDH[a]	Soundings, DU	Microtops II, DU
9808111205	306 ± 21[b]	not available
9906030933	326 ± 23	337 ± 13
9906031204	328 ± 23	320 ± 13
9906040705	320 ± 22	354 ± 14
9906041519	320 ± 22	305 ± 12
9906050639	330 ± 23	346 ± 14
0006290934	282 ± 20	296 ± 12
0006291205	327 ± 23	302 ± 12

[a]YMDH, year, month, day, hour; read 9808111205 as 11 August 1998, 1205 UT.
[b]Sounding carried out in Madrid (200 km from Barrax).

circumsolar radiation would probably be slightly less, and so too the inaccuracy due to this radiation.

[23] From values of the spectral AOD it is possible to obtain different related parameters, particularly the atmospheric turbidity. Different atmospheric turbidity indexes have been developed with the aim of studying the aerosol radiative effects, the Angstrom turbidity coefficient being the most frequently used. *Angstrom* [1929] proposed the following parameterization

$$\tau_a(\lambda) = \beta\lambda^{-\alpha}, \tag{2}$$

where the wavelength is expressed in micrometers. The coefficient β, known as the turbidity coefficient, represents the atmospheric aerosol content (and is equal to $\tau_{a\lambda}$ at 1000 nm), and the α coefficient, known as the wavelength exponent, is related to the aerosols' size. The α parameter has been the subject of numerous papers over the past 20 years in relation to its application in remote sensing. Since many satellite-based and ground-based measurements provide retrievals of spectral AOD but no direct size distribution retrievals, the analysis of α is important for the interpretation of these data and to provide further information on particle size [*Eck et al.*, 2001b]. Lately, the Angstrom-type parameterization has acquired renewed interest thanks to the recent work of *O'Neill et al.* [2001, 2002] in which a new formalism based on the geometric interpretation of the AOD curves against the wavelength is developed from the formulation by *Shifrin* [1995].

[24] Since Angstrom proposed equation (2) it has been used enormously for parameterizing the spectral values of the AOD derived from the measurements obtained with Sun photometers and spectroradiometers. From the spectral values of AOD it is possible to determine the Angstrom coefficients using three different procedures [*Cachorro et al.*, 1987a]: (1) The *Volz* [1959] method, which consists in applying equation (2) to photometer measurements made in two different narrow wavelength bands, (2) the direct method, which consists in obtaining α as the negative of the derivative of the AOD with respect to ln λ, (3) linear fitting, consisting in linearly fitting equation (2) in double logarithm form through the following equation:

$$\ln\tau_a(\lambda) = -\alpha\ln\lambda + \ln\beta. \tag{3}$$

[25] *Cachorro et al.* [1987a] show that when the Volz method is applied, large variations in the value of α are obtained especially when nearby wavelengths are used. Similar results have been obtained by *Utrillas et al.* [2000] when this method is used for direct irradiance measures in the broad band using filters. Various authors [*Cachorro et al.*, 1987b; *Bokoye et al.*, 1997] have tried to establish an optimum pair of wavelengths for applying the Volz method, with contradictory results. It would appear that the optimum pair depends on the instruments, the spectral range and the resolution used, as well as the atmospheric conditions and the solar altitude [*Bokoye et al.*, 1997]. The direct method is, in turn, associated with big intrinsic inaccuracies, being based on the derivative of a set of discrete points. In this case it has been shown that the value of α depends both on the size of the $\Delta\lambda$ used and on the limits of the same [*Cachorro et al.*, 1987a].

[26] The logarithmic lineal fit, given in equation (3) is the least imprecise, although the results that it gives can also depend on the spectral interval considered [*Cachorro et al.*, 2000a, 2000b; *Martínez-Lozano et al.*, 2001; *Eck et al.*, 1999, 2001a; *Smirnov et al.*, 2003]. Nevertheless, equation (3) has been used by many authors over the years and is currently used to parameterize the AOD values derived from the Aerosol Robotic Network (AERONET) program [*Holben et al.*, 1998, 2001].

[27] On the other hand, to quantify the curvature of τ_a *Eck et al.* [1999] propose using the second derivative of ln τ_a versus ln λ, related to the derivative of α with respect to the ln λ. From equation (2) and the second-order polynomial fit given by equation (4):

$$\ln\tau_a = a_0 + a_1\ln\lambda + a_2(\ln\lambda)^2 \tag{4}$$

the following relation is obtained:

$$\alpha' = \frac{d\alpha}{d\ln\lambda} = -\frac{d\left(d\ln\tau_a/d\ln\lambda\right)}{d\ln\lambda} = -2a_2. \tag{5}$$

[28] We have applied the values of the spectral AOD to both the logarithmic lineal fit, given in equation (3), as well as the analysis of the derivative of the wavelength exponent proposed by *Eck et al.* [1999].

5. Results and Discussion

[29] The spectral AOD was obtained from extinction measurements of solar direct irradiance by applying Beer's law, following the procedure described in the previous section. In this way, for each spectral direct solar irradiance measurement set, 270 values of AOD were obtained for the spectral range 400–670 nm. To perform a complete sweep in this spectral range the Licor 1800 takes 27 s and the Optronics takes 60 s. During the DAISEX-98 campaign the Optronic 754 was not available. For this reason and to guarantee homogeneity of the results for the three DAISEX campaigns, the data presented here were all obtained from data acquired with the Licor 1800. The results available from the Optronics have been used to validate the results from the Licor. As we have already indicated, the deviations between the values given by both instruments are less than 2% [*Martínez-Lozano et al.*, 2003]. However, the errors affecting these results are greater in the case of the Licor,

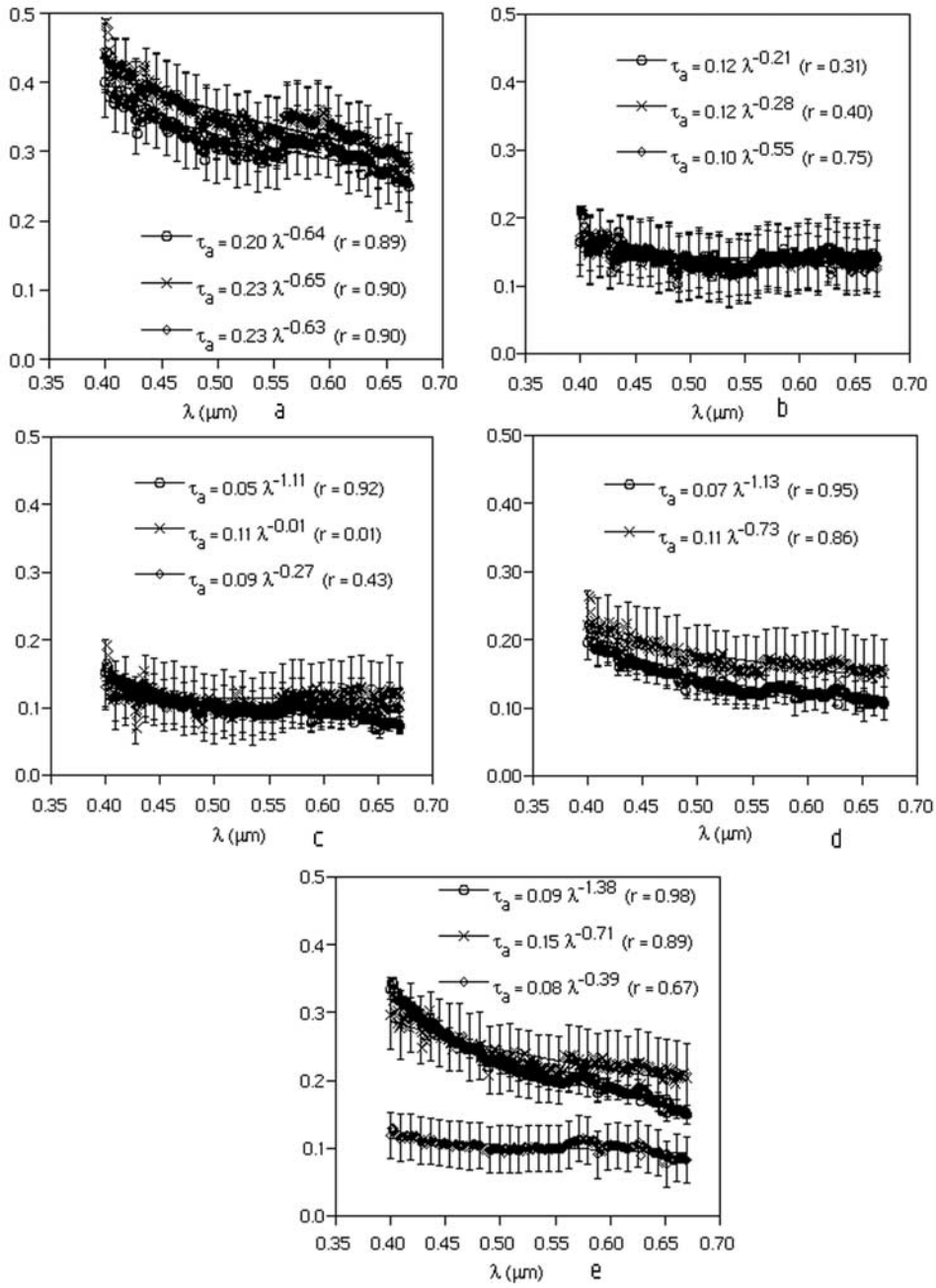

Figure 9. AOD at Barrax in the range 400–670 nm. (a) 11 August 1998: dots, 1036 UTC; crosses, 1200 UTC; diamonds, 1318 UTC. (b) 3 June 1999: dots, 1115 UTC; crosses, 1200 UTC; diamonds, 1500 UTC. (c) 4 June 1999: dots, 0605 UTC; crosses, 1200 UTC; diamonds, 1600 UTC. (d) 5 June 1999: dots, 0700 UTC; crosses, 1000 UTC. (e) 29 June 2000: dots, 0600 UTC; crosses, 1200 UTC; diamonds, 1600 UTC.

due to its larger FWHM. These errors are the ones considered in the analysis of the results.

[30] Figures 9a–9e show, for each campaign day, the AOD values for solar noon and the first and last measurements made each day. The time of the latter are not fixed since the ground measurements had to coincide with the flight times of the planes that took part in the campaign. For the spectral AOD obtained for each measurement set, the α and β Angstrom parameters were calculated using a direct fit of equation (2) in the visible band (400–670 nm). As an example, in the same Figures 9a–9e, the fits corresponding to each of the sets of spectral AOD values of each figure are also shown. In Table 4 the mean daily values of the α and β fitted coefficients are shown. This table also includes the average daily values of AOD for 500 nm (τ_{500}), the value usually used to characterize the aerosols in the AERONET network [*Holben et al.*, 2001; *Smirnov et al.*, 2002]. Each parameter has associated with it the standard deviation (σ_i), obtained from the different values available for each day (shown by n in Table 4). The results for α show a high variability in the aerosol size, especially on 29 June 2000 and 4 June 1999, with values of σ of the order of 50 and

Table 4. Daily Mean Values of AOD for 500 nm (τ_{500}), α and β Angstrom Coefficients in the Range 400–670 nm[a]

YMD[b]	τ_{500}	σ_τ	α	σ_α	β	σ_β	n	r (Minimum)	r (Maximum)
980811	0.34	0.02	0.66	0.03	0.22	0.01	8	0.89	0.92
990603	0.13	0.01	0.31	0.01	0.12	0.04	16	0.31	0.75
990604	0.10	0.01	0.38	0.44	0.09	0.03	41	0.00	0.94
990605	0.16	0.03	0.91	0.13	0.09	0.02	13	0.82	0.95
000629	0.20	0.04	0.85	0.22	0.12	0.03	39	0.69	0.98

[a]σ_i, Standard deviation; n, number of measurements over a day; r, correlation coefficient.
[b]YMD, year, month, day.

115%, respectively. Given that Table 4 shows the average values over the length of a day it is not possible to assign to each of them a value for the correlation coefficient, r, of the Angstrom fit. Instead, the range of variation of r is given for each measurement day.

[31] In Figures 9a–9e can be seen the change in the slope in the experimental values of the spectral AOD at around the 550-nm wavelength. This change of slope is particularly noticeable in Figure 9a, corresponding to 11 August 1998, but to a greater or lesser extent is present in all the spectral AOD curves obtained experimentally. There are three possible explanations of this discontinuity: (1) measurement errors due to misalignments of the instruments at the time and in the spectral range considered, (2) errors in the methodology used to derive the spectral AOD from spectral extinction measurements of direct irradiance, (3) a real discontinuity in the spectral value of AOD, such that it does not follow Angstrom's Law which has been considered valid a priori for this spectral interval. We briefly analyze each of these possibilities.

[32] The Licor 1800 spectroradiometers used in these campaigns are periodically submitted to a double-calibration process. They are calibrated indoors with a laboratory reference lamp and also intercompared outdoors with other instruments with different characteristics in the same spectral range [*Alados-Arboledas et al.*, 2003; *Martínez-Lozano et al.*, 2003; *Sánchez-Muniosguren et al.*, 2003]. The results of these intercomparisons with the other spectroradiometers of greater precision (Optronic or Bentham) show that the Licor 1800 are particularly well suited for the measurement of the extinction of direct irradiance in the visible range [*Martínez-Lozano et al.*, 2003], so any systematic error in the measurement process can be disregarded. As for the methodology followed to obtain the AOD, once the total atmospheric optical depth was obtained using Beer's Law, it only consists in correcting the experimental values for Rayleigh and ozone. Given that Rayleigh scattering is continuous with respect to wavelength, it remains to consider the ozone correction as a possible source of error, since the absorption of the Chappuis band acquires more importance above the 550-nm wavelength. To eliminate possible errors due to this cause, a thorough revision of the calculations has been performed in which consideration has also been given to the small H_2O absorption bands present in this spectral interval.

[33] Moreover, this discontinuity in the curvature of the spectral AOD has also been detected in previous campaigns carried out in other locations, using different instruments [*Martínez-Lozano et al.*, 2001]. We therefore consider that the justification of this effect must be based on the optical properties of the aerosols that are only manifest when working with high-spectral-precision spectroradiometers. Such optical properties would be difficult to detect when using sunphotometers with a limited number of bands, as is the case for example of certain models of CIMEL sunphotometers used in the AERONET network that only have two measurement bands in the spectral range 440–670 nm. Nevertheless, even in this case, we can often find AOD spectral curves obtained with several types of sunphotometers where the discontinuity appears not necessarily in the same wavelength as in these campaigns [see, for example, *Moorthy et al.*, 2003; *Smirnov et al.*, 2003].

[34] In our opinion the change in curvature in spectral AOD could be due to the fact that normally there is more than one type of aerosol simultaneously present in the atmosphere, so characterizing them using a single value of the Angstrom α is only a first approximation. *Shifrin* [1995] starting from the Mie theory and the Angstrom formula shows theoretically that in the presence of various types of aerosols (identified by i) the following relation holds:

$$\alpha = \Sigma\alpha_i(\tau_{ai}/\tau_a) \qquad \tau_a = \Sigma\tau_{ai}, \tag{6}$$

[35] *O'Neill et al.* [2001] have applied this relation to a bimodal distribution (fine and coarse), obtaining a series of relations that give aerosol optical properties with bimodal distributions. Our group is currently working on an alternative to the O'Neill approach, based not on the geometry of the AOD curve but on the Mie theory. This approach uses inversion methods and aerosol microphysical properties to determine the spectral contribution to the aerosol optical thickness due to each type of aerosols. The main difference between our methodology and the geometrical approximation of *O'Neill et al.* [2001], apart from the mathematical algorithms used, is that we aim to determine the types of aerosols, whereas O'Neill et al. focus on determining the aerosols in the fine and coarse mode of the bimodal distribution, without taking into account their origin. This alternative approach assumes that a concrete type of aerosol can contribute (with different relative weight) to both modes of the bimodal distribution. This approach is currently under development [*Gómez-Amo et al.*, 2002].

[36] In the light of this AOD experimental curvature change, we chose to consider two subintervals in the visible range and to make two independent adjustments to equation (2). The subintervals chosen were 400–550 and 550–670 nm. Figures 10a–10e show similar fits to those presented in Figures 9a–9e but limited to the 400–550 nm spectral range. The mean daily adjustment parameters corresponding to these subintervals are shown in Tables 5 and 6, respectively. For the 400–550 nm spectral range (Table 5) it can be seen that in all cases the correlation coefficient improved noticeably while at the same time the variability of α reduced significantly. In the 550–670 nm interval (Table 6) the values for α that were obtained are typical of big particles in the coarse mode, which appears to indicate greater influence from these coarse particles in this spectral interval. In view of the back trajectories analyzed above, these values could be associated with sea salt particles of radius $\sim$2 μm.

[37] Figures 11a–11e show the daily evolution of the τ_{500} and the Angstrom parameters (in the 400–550 nm range) for the 5 campaign days. The day corresponding to DAISEX-98

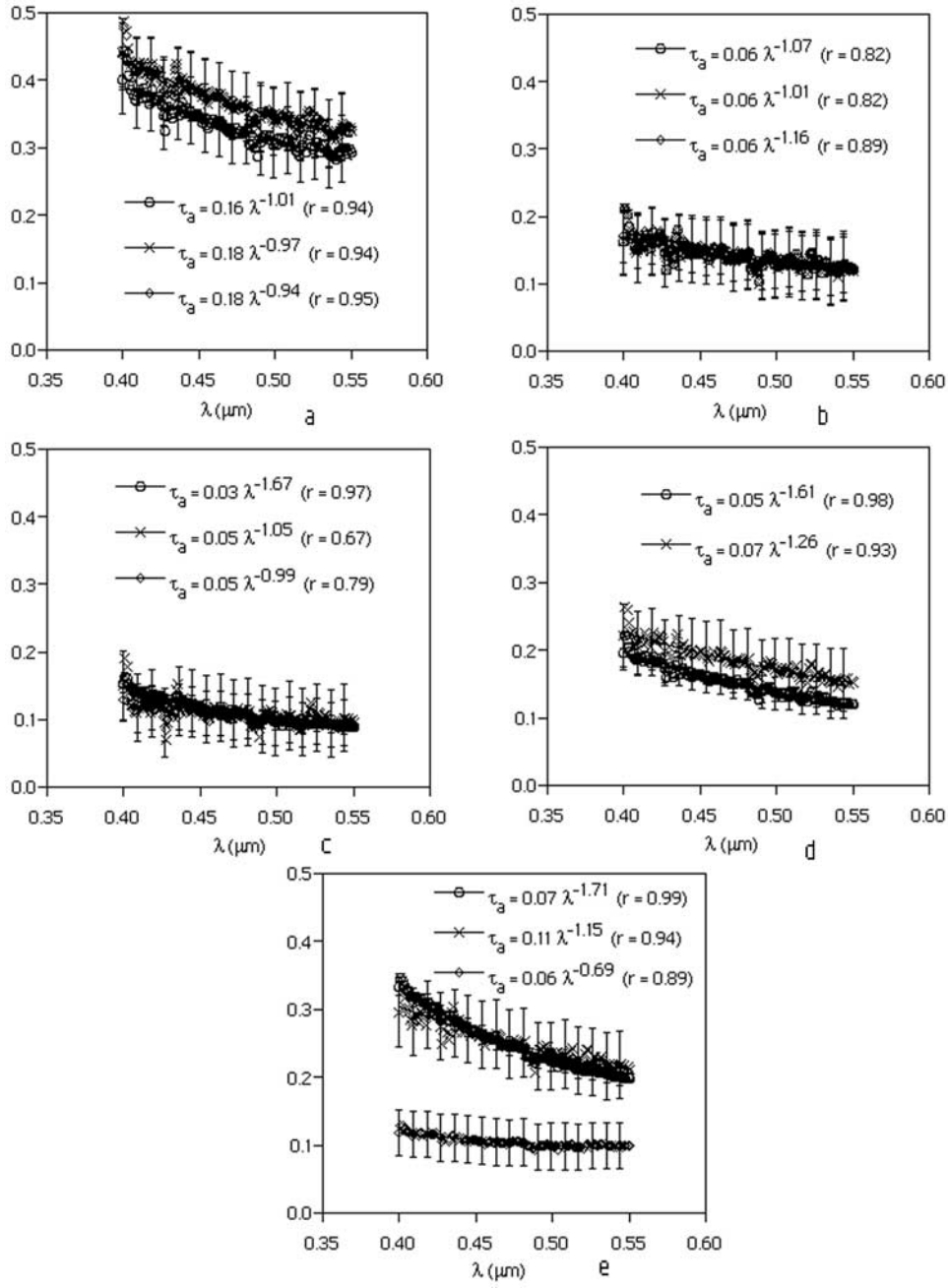

Figure 10. AOD at Barrax in the range 400–550 nm. (a) 11 August 1998: dots, 1036 UTC; crosses, 1200 UTC; diamonds, 1318 UTC. (b) 3 June 1999: dots, 1115 UTC; crosses, 1200 UTC; diamonds, 1500 UTC. (c) 4 June 1999: dots, 0605 UTC; crosses, 1200 UTC; diamonds, 1600 UTC. (d) 5 June 1999: dots, 0700 UTC; crosses, 1000 UTC. (e) 29 June 2000: dots, 0555 UTC; crosses, 1159 UTC; diamonds, 1600 UTC.

Table 5. Daily Mean Values of α and β Angstrom Coefficients in the Range 400–550 nm[a]

YMD[b]	α	σ_α	β	σ_β	n	r (Minimum)	r (Maximum)
980811	1.00	0.04	0.17	0.01	8	0.94	0.95
990603	1.06	0.09	0.06	0.01	16	0.80	0.89
990604	1.32	0.41	0.04	0.01	41	0.59	0.98
990605	1.45	0.12	0.06	0.02	13	0.93	0.98
000629	1.24	0.22	0.09	0.02	39	0.81	0.99

[a]σ_i, Standard deviation; n, number of measurements over a day; r, correlation coefficient.
[b]YMD, year, month, day; read 980811 as 11 August 1998.

Table 6. Daily Mean Values of α and β Angstrom Coefficients in the Range 550–670 nm[a]

YMD[b]	α	σ_α	β	σ_β	n	r (Minimum)	r (Maximum)
980811	1.02	0.03	0.19	0.01	8	0.83	0.86
990603	−0.17	0.14	0.15	0.01	16	0.02	0.89
990604	−0.09	0.40	0.11	0.03	41	0.02	0.73
990605	0.52	0.29	0.12	0.03	13	0.20	0.93
000629	0.70	0.27	0.13	0.03	39	0.32	0.92

[a]σ_i, Standard deviation; n, number of measurements over a day; r, correlation coefficient.
[b]YMD, year, month, day; read 980811 as 11 August 1998.

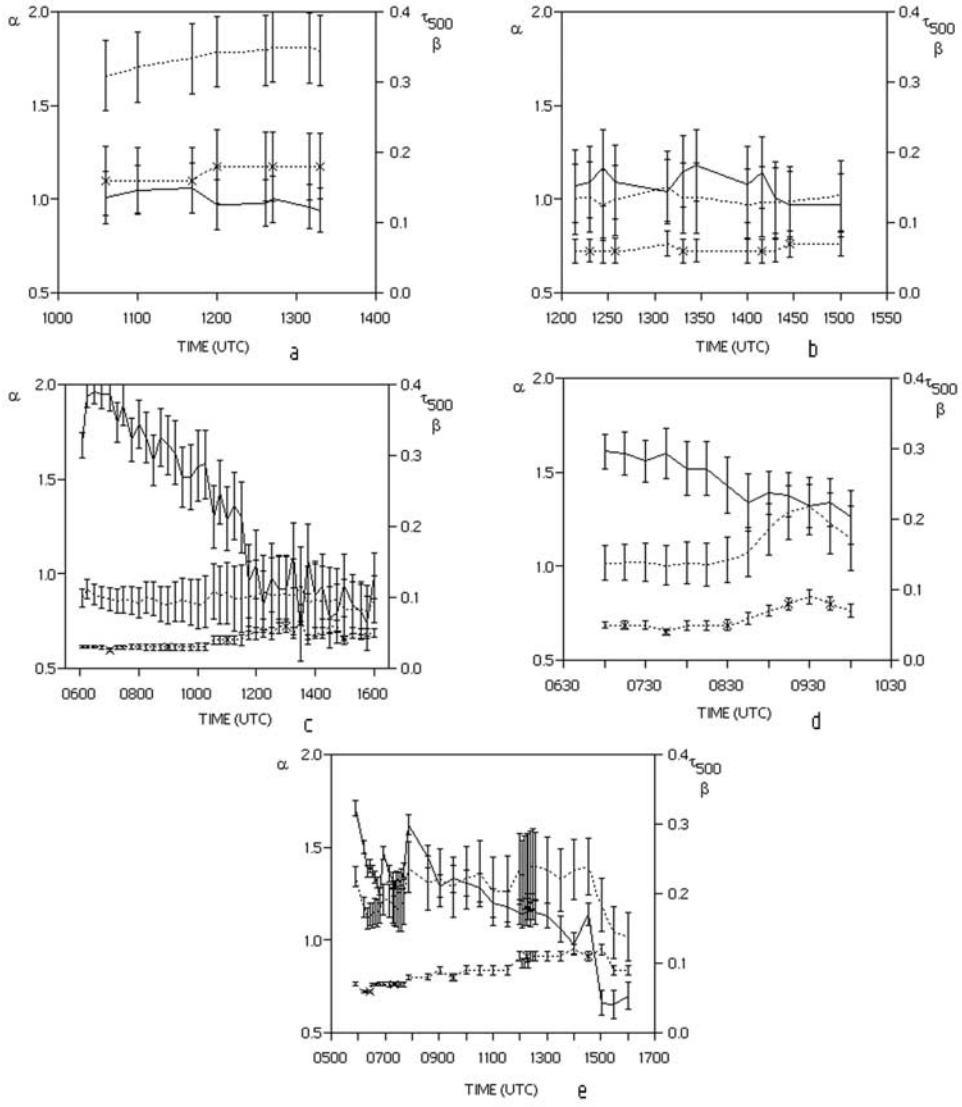

Figure 11. Daily evolution of τ_{500} (dashed line), α (solid line) in the range 400–550 nm and β (dashed line with crosses) at Barrax: (a) 11 August 1998; (b) 03 June 1999; (c) 04 June 1999; (d) 05 June 1999; and (e) 29 June 2000.

(11 August 1998, Figure 11a) showed stability in relation to the quantity and type of aerosols, as already shown by the low standard deviation values in Tables 4 and 5. On this day τ_{500} remained between 0.30 and 0.35, and the Angstrom parameters in the ranges 0.95–1.05 (α) and 0.16–0.18 (β). The days corresponding to the DAISEX-99 campaign (Figures 11b–11d) were characterized by very small aerosols with relatively stable values of τ_{500} in the ranges 0.13–0.15, 0.09–0.12, and 0.15–0.22, for the June days 3, 4, and 5, respectively. It can be seen how the effect of previously mentioned rain front became gradually less from day to day. The α values presented great variability, showing two apparently conflicting trends: (1) an increase in the average daily value over the campaign and (2) a daily decrease over the length of each day. This could be explained by two complementary effects: (1) a reduction in size over the 3 days due to a greater contribution from continental-type particles in lower atmospheric levels, which initially were scarce due to the passage of the rain front (at least in the accumulation nucleus which has greatest weight in the wavelength range that we were considering, 400–550 nm) and (2) an increase in size over the length of each day. In view of the radiosondes for these days the second effect cannot be explained on the basis of hygroscopic effects; it is more likely to be an effect of anthropogenic activity (the measurement period coincides with the harvest time in the measurement zone). Finally, for the DAISEX-2000 campaign (Figure 11e) a situation similar to that described for the DAISEX-99 campaign was found with values of τ_{500} similar to those of the last day of that campaign, but with a much more marked variation in α over the length of the day.

[38] To quantify the curvature of τ_a [*Eck et al.*, 1999], we determined the values of a_2 from each of the series of values of τ_a in the ranges 400–670 and 400–550 nm (Figure 12). Table 7 shows for each day the average value corresponding to α', as well as the corresponding standard deviation. According to *Eck et al.* [1999], large positive values of α'

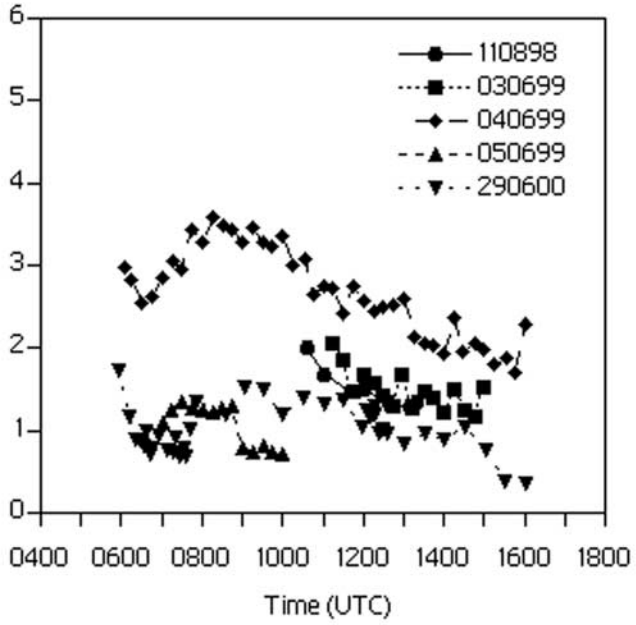

Figure 12. Values of the coefficient a_2 of the second-order polynomial $\ln \tau_a = a_0 + a_1 \ln \lambda + a_2 (\ln \lambda)^2$. Range 400–550 nm.

are characteristics of fine-mode-dominated aerosol size distribution, while near-zero and negative values of α' are characteristics of bimodal distributions with the coarse mode having a significant relative magnitude. Following this criterion for our case there was a clear predominance of the coarse mode over the accumulation mode for all the days of the measurement campaign.

[39] Figures 9a–9e and 10a–10e and Tables 4–6 allow us to analyze the AOD for each of the days of the measurement campaign. When we consider the whole spectral range corresponding to the visible range (400–670 nm), the results from the DAISEX-98 campaign (11 August 1998; Figure 9a) showed correlation coefficients around 0.9 and stable values for α and β throughout the day. The values of β, approximately 0.2, were on the order of the values considered as medium turbidity conditions at this region for the summer. The values of α of about 0.65 were indicators of the presence of large-sized particles. For the DAISEX-98 campaign the back trajectories show that the air masses in the different layers have different origins (Figure 5a). Thus the trajectory of the lower layers is associated with a thermal low over the Peninsula that sucks air in from the surroundings, which, for the measurement site, is air of Mediterranean origin (this is also explained in part by the existence of breezes but only at the end of the back trajectory). The trajectory at around 2000 m corresponds to a weak flow, predominantly from north. Finally, the back trajectory at 3000 m above ground level reflects the situation at higher levels in which the very weak westerly winds predominate. It is therefore to be expected that the aerosols present are the result of a combination of maritime aerosols at high levels and rural continental aerosols at medium and low levels. The presence of rural continental aerosols would seem to be increased also by the fact that the back trajectories at the 500 m level reach the surface. The spectral AOD curves (Figures 9a and 10a) seem to confirm this fact. The curve is more peaked at the lower wavelengths, which means that, as well as maritime aerosols, there are continental aerosols [*O'Dowd and Smith*, 1993; *Moorthy et al.*, 2003].

[40] For the DAISEX-99 campaign (3, 4, and 5 June 1999; Figures 9b–9d and 10b–10d) the results showed greater variability over the length of the day. Most notable were the low values of AOD, which could be explained by the fact that on the previous days a cold Atlantic weather front had passed over the measurement site, accompanied by rain which effectively "cleaned" the atmosphere. This atmospheric clearness was also reflected in the values of the β coefficient, which normally would not pass the value of 0.10 for the 3 days of the campaign. The DAISEX-99 days were also characterized by presenting big variations in the value of the wavelength exponent. For the DAISEX-99 campaign, in view of the back trajectories shown in Figures 5b–5d, it would appear that there was a combination of aerosols of Atlantic maritime origin [*Smirnov et al.*, 2002, 2003] with continental aerosols, whose relative weight increased as the effect of the rain front decreased (α increases as the days pass). On these days the contact with the ground by the air masses corresponding to the back trajectories at the 500 m is even more persistent than for the DAISEX-98 campaign. This translated into a decrease in the relative importance of the coarse-particle mode with respect to the fine-particle mode and into an increase in the average daily value of α.

[41] For the DAISEX-2000 campaign (29 June 2000; Figure 9e) the results of the fits showed higher correlation coefficients. This day showed low values of β (on the same order as those obtained for 1999) and a sharp evolution of α over the day from 1.38 to 0.39. This could be explained in the light of the back trajectories in Figure 5e in which we see that the air masses at different heights all originated from high strata over the Atlantic, over which they had traveled large distances. In particular, the back trajectory corresponding to 500 m above sea level showed an air mass that 16 hours earlier had been still over the ocean at a height of 2500 m above sea level.

[42] If we compare the results obtained for the two spectral ranges we see that during the DAISEX-99 and DAISEX-2000 campaigns a reduction of the spectral range toward the shorter wavelengths implied a decrease in the absolute value of α', especially during the days in 1999. Nevertheless, the values of α' are still negative at shorter wavelengths, so the coarse mode still dominates. On the other hand, in the DAISEX-98 campaign the reduction of

Table 7. Daily Mean Value of α' as Well as the Corresponding Standard Deviation

	Range 400–670		Range 400–550		
YMD[a]	α'	σ	α'	σ	n
980811	−1.1	0.2	−3.0	0.5	8
990703	−5.4	0.7	−3.0	0.45	16
990704	−6.5	1.4	−5.2	1.1	41
990704	−4.2	0.6	−2.1	0.5	13
000629	−2.6	0.6	−2.0	0.6	39

[a]YMD, year, month, day; read 980811 as 11 August 1998.

the spectral interval translated into an increase in the influence of the coarse mode, which indicated that during this day the aerosols present were of a different type.

[43] The comparison of our results with the ones provided by AERONET network has only been possible for 2000. The closest station to our measurement site is El Arenosillo (37°N, 6°W, 0 m a.s.l., 500 km to the southeast). The Azores station (38°N, 28°W), though 2000 km to the west, is also interesting as the air masses pass over it in their way to the measurement site. Unfortunately, during the days of the DAISEX campaigns only the data for the year 2000 are available on the Internet for the above mentioned stations. On 29 June 2000, the τ_{a440} for El Arenosillo is 0.085 and for Azores (48 hours before) is 0.061. The values of α for such stations, using 440 and 670 nm, are 1.1 for El Arenosillo and 1.0 for Las Azores (always 48 hours before). These values differ considerably from those of Barrax, 0.22 for τ_{a440} and 0.85 for α. We could explain the highest AOD value for Barrax in the base of a stronger contribution of the continental air masses as they have crossed the Iberian Peninsula. The difference in α is more complicated to explain as its decrease compared to the AERONET stations contradicts the possible contribution due to the continental aerosols that would explain the increase in τ_{a440}. Nevertheless and taking into account the back trajectories, if we admit that aerosols over the measurement site have an Atlantic origin, the values for Barrax are coherent with the climatic values of AERONET network. Those values are 0.14 for τ_{a500} for mixed maritime aerosols and 0.62–0.93 for α [*Smirnov et al.*, 2002].

6. Concluding Remarks

[44] The spectral AOD was obtained from extinction measurements of solar direct irradiance (270 values for the spectral range 400–670 nm) for the different days of the ESA DAISEX campaigns. From the spectral AOD obtained for each measurement set, the α and β Angstrom parameters were calculated using a direct fit in the visible band. The results show a change in the slope in the experimental values of the spectral AOD at around the 550-nm wavelength. This change could be due to the fact that normally there are simultaneously present in the atmosphere more than one type of aerosols, so characterizing them using a single value of the Angstrom α is only a first approximation.

[45] In the light of this AOD experimental curvature change, we chose to consider two subintervals in the visible range, 400–550 and 550–670 nm. For the 400–550 nm spectral range the variability of α significantly reduced. In the 550–670 nm interval the values for α that were obtained are typical of big particles in the coarse mode, which appears to indicate greater influence from these coarse particles in this spectral interval. The analysis of the wavelength exponent α showed a high dependence on the spectral range used. The uncertainties decreased if we limited its determination to the 400–550 nm range, although in this case information was lost on the aerosols in the coarse particle mode.

[46] The results for the measurement day set show that in all cases the coarse-particle mode was dominant over the fine-particle mode. These results, obtained basically from the values of α', were sensitive to the spectral interval considered. This suggests a future research line in which the contribution from the two modes as a function of the value of α' and the spectral interval could be quantified.

[47] Overall, the results obtained showed that during the DAISEX there was a combination of maritime aerosols and smaller continental aerosols. The analysis of the back trajectories of the air masses indicated a predominance of maritime-type aerosols in all atmospheric layers, although from two distinct sources: the Atlantic and the Mediterranean. When the surface air masses came from the Mediterranean they combined with continental air masses at altitude, giving rise to an increase in the value of the AOD. These results confirmed the need to use back trajectories to identify the aerosols over a particular site: Barrax, for instance, is 200 km from the Mediterranean Sea and 800 km from the Atlantic Ocean.

[48] The comparison of the results obtained during the campaign with those available from the AERONET network show a very weak correlation. AERONET is a very useful tool for analyzing the spatial distributions of aerosols at a planetary level as well as for establishing a climatology of them. However, in order to determine specific applications, such as the atmospheric correction of remote sensing campaign data, in situ measurements of extinction are desirable.

Appendix A. Acronym List

[49] AERONET: Aerosol Robotic Network

[50] AOD: Aerosol Optical Depth

[51] ARAT: Avion de Recherche Atmosphérique et de Télédéction

[52] CNES: Centre National d'Etudes Spatiales

[53] CNRES: Centre National de la Recherche Scientifique

[54] DAIS: Digital Airborne Imager Spectrometer

[55] DAISEX: Digital Airborne Imaging Spectrometer Experiment

[56] DLR: Deutche Forschungsanstalt für Luft und Raumfahrt

[57] ECMWF: European Centre for Medium range Weather Forecasting

[58] EFEDA: European International Project on Climatic and Hydrological Interactions between Vegetation, Atmosphere and Land Surface, Field Experiment in Desertification Threatened Areas

[59] ESA: European Space Agency

[60] FOV: Field Of View

[61] FWHM: Full-Width at Half-Maximum

[62] HIRLAM: High-Resolution Limited Area Model

[63] HYMAP: Hyperspectral Mapping

[64] HYSPLIT: Hybrid Single-Particle Lagrangian Integrated Trajectory

[65] INM: Instituto Nacional de Meteorología

[66] IGN: Institut Geographique National

[67] INSU: Institut National des Sciences de l'Univers

[68] LEANDRE: Lidar Embarqué Pour l'Etude des Aerosols et des Nuages, de l'Interaction Dynamique-Rayonnement et du Cycle de l'Eau

[69] LSPIM: Land Surface Processes and Interactions Mission

[70] MERIS: Medium-Resolution Imaging Spectrometer

[71] POLDER: Polarization and Directionality of the Earth's Reflectance

[72] ROSIS: Reflective Optics System Imaging Spectrometer

[73] SKYRAD.PACK: Inversion Radiative Transfer Software Package to Analyze Sky Radiation for the Study of the Aerosol Remote Sensing

[74] SMARTS2: Simple Model of the Atmosphere Radiative Transfer of Sunshine

[75] SPECTRA: Surface Processes and Ecosystem Changes Through Response Analysis

[76] STAAARTE: Scientific Training and Access to Aircraft for Atmospheric Research Throughout Europe

[77] UTC: Coordinated Universal Time

[78] **Acknowledgments.** The DAISEX campaigns were financed by funds from the European Space Agency (ESA), and currently R. Pedrós holds a grant from ESA to process the data obtained during these campaigns. The authors would like to thank the members of all the groups participating in DAISEX in Barrax for their collaboration, especially J. Moreno, the coordinator of the team who brought together the different Spanish working groups. The authors wish to thank J. Tamayo of the Centro Meteorológico Zonal de Levante del INM for his valuable comments on the interpretation of synoptic meteorological maps and the back trajectories of air masses. The authors acknowledge the SIMBIOS Project at NASA Flight Goddard Center and the principal investigator of the El Arenosillo site Victoria Cachorro Revilla for supplying the AERONET data. The authors thank two anonymous reviewers for their helpful comments on the manuscript.

References

Alados-Arboledas, L., et al., VELETA 2002 field campaign, *Geophys. Res. Abstr.*, *5*, 12,218, 2003.

Anderson, S. M., and K. Mauersberger, Measurements of ozone absorption cross section in the Chappuis band, *Geophys. Res. Lett.*, *19*, 933–936, 1992.

Angstrom, A., On the atmospheric transmission of sun radiation and on the dust in the air, *Geogr. Ann.*, *11*, 156–166, 1929.

Berger, M., J. Moreno, A. Mueller, M. Schaepman, P. Wursteisen, M. Rast, and E. Attema, The Digital Airborne Imaging Spectrometer Experiment—DAISEX'99, *Proc. IGARSS 2000*, Ed. IEEE, pp. 3039–3041, 2000.

Berger, M., et al., The DAISEX campaigns in support of a future land surface processes mission, *ESA Bull.*, *105*, 101–111, 2001.

Bodhaine, B. A., N. B. Wood, E. G. Dutton, and J. R. Slusser, On Rayleigh optical depth calculations, *J. Atmos. Oceanic Technol.*, *16*, 1854–1861, 1999.

Bokoye, A. I., A. de la Casinière, and T. Cabot, Angstrom turbidity parameters and aerosol optical thickness: A study over 500 solar beam spectra, *J. Geophys. Res.*, *102*, 21,905–21,914, 1997.

Bolle, H. J., et al., EFEDA: European field experiment in a desertification-threatened area, *Ann. Geophys.*, *11*, 173–189, 1993.

Cachorro, V. E., A. M. Frutos, and J. L. Casanova, Determination of the Angstrom turbidity parameters, *Appl. Opt.*, *26*, 3069–3076, 1987a.

Cachorro, V. E., A. M. Frutos, and J. L. Casanova, The influence of Angstrom turbidity parameters on calculated direct solar spectral irradiance at high turbidity, *Sol. Energy*, *39*, 399–407, 1987b.

Cachorro, V. E., P. Durán, R. Vergaz, and A. De Frutos, Columnar physical and radiative properties of atmospheric aerosols in north central Spain, *J. Geophys. Res.*, *105*, 7161–7175, 2000a.

Cachorro, V. E., P. Durán, R. Vergaz, and A. De Frutos, Measurements of the atmospheric turbidity of the north-centre continental area in Spain: Spectral aerosol optical depth and Angstrom turbidity parameters, *J. Aerosol Sci.*, *31*, 687–702, 2000b.

Chang, S. H., M. J. Westfield, F. Lehmann, D. Oertel, and R. Richter, 79-channel airborne imager spectrometer, *SPIE*, *1937*, 164–172, 1993.

Cocks, T., R. Jenssen, A. Stewart, I. Wilson, and T. Shields, The HYMAP airborne hyperspectral sensor: The system, calibration and performance, paper presented at First EARSeL Workshop on Imaging Spectroscopy, Zurich, Eur. Assoc. of Remote Sens. Lab., Paris, 1998.

Deschamps, P. Y., F. M. Bréon, M. Leroy, A. Podaire, A. Bricaud, J. C. Buriez, and G. Sèze, The POLDER mission: Instrument characteristics and scientific objectives, *IEEE Trans. Geosci. Remote Sens.*, *32*, 598–615, 1994.

Eck, T. F., B. N. Holben, J. S. Reid, O. Dubovik, A. Smirnov, N. T. O'Neill, I. Slutsker, and S. Kinne, Wavelength dependence of the optical depth of biomass burning, urban and desert dust aerosols, *J. Geophys. Res.*, *104*, 31,333–31,349, 1999.

Eck, T. F., B. N. Holben, D. E. Ward, O. Dubovik, J. S. Reid, A. Smirnov, M. M. Mukelabai, N. C. Hsu, N. T. O'Neill, and I. Slutsker, Characterization of the optical properties of biomass burning aerosols in Zambia during the 1997 ZIBBEE field campaign, *J. Geophys. Res.*, *106*, 3425–3448, 2001a.

Eck, T. F., B. N. Holben, O. Dubovik, A. Smirnov, I. Slutsker, J. M. Lobert, and V. Ramanathan, Column-integrated aerosol optical properties over the Maldives during the northeast monsoon for 1998–2000, *J. Geophys. Res.*, *106*, 28,555–28,566, 2001b.

Estellés, V., M. P. Utrillas, J. L. Gómez-amo, R. Pedrós, and J. A. Martinez-Lozano, Aerosol size distributions and air mass backtrajectories over a Mediterranean coastal site, *Int. J. Remote Sens.*, *24*, 1–12, 2003.

European Space Agency (ESA), Reports for mission selection, in *The Four Candidate Earth Explorer Core Missions: Land-Surface Processes and Interactions*, *ESA SP-1233* (*2*), ESA Publ. Div., ESTEC, Netherlands, 1999.

European Space Agency (ESA), *DAISEX* (*Digital Airborne Imaging Spectrometer Experiment*), ESA Publ. Div., ESTEC, Netherlands, 2001a.

European Space Agency (ESA), Reports for assessment, in *The Five Candidate Earth Explorer Core Missions: SPECTRA—Surface Processes and Ecosystems Changes Through Response Analysis*, *ESA SP-1257* (*5*), ESA Publ. Div., ESTEC, Netherlands, 2001b.

Flamant, C., and J. Pelon, Atmospheric boundary-layer structure over the Mediterranean during a Tramontane event, *Q. J. R. Meteorol. Soc.*, *122*, 1741–1778, 1996.

Gege, P., and W. Mooshuber, Electronic performance of the imaging spectrometer ROSIS-03, in *Proceedings of the Workshop of ISPRS, Working Groups I/1, i/3 and IV/4: Sensors and Mapping From Space*, pp. 49–67, Univ. of Hanover, Hanover, 1997.

Gómez-Amo, J. L., M. P. Utrillas, V. Estellés, R. Pedrós, and J. A. Martínez-Lozano, A new approach to characterize aerosols from their optical depth spectral values: Simulated case study, in *Recent Advances in Quantitative Remote Sensing*, edited by J. Sobrino, pp. 100–107, Univ. of Valencia, Valencia, 2002.

Gonzalez, M. C., J. C. Fortea, J. A. Martínez-Lozano, M. P. Utrillas, R. Pedrós, J. Moreno, J. M. Cisneros, and J. L. Manzano, Measurements of atmospheric constituents (ozone, water vapour) at Barrax in DAISEX-1998, DAISEX-1999 and DAISEX-1999 extension, in *DAISEX Final Results Workshop*, pp. 53–62, ESA Pub. Div., ESTEC, Netherlands, 2001.

Gueymard, C. A., Parameterized transmittance model for direct beam and circumsolar spectral irradiance, *Sol. Energy*, *71*, 325–346, 2001.

Holben, B. N., A. Setzer, T. F. Eck, A. Pereira, and I. Slutsker, Effect of dry season biomass burning on Amazon basin aerosol concentrations and optical properties, 1992–1994, *J. Geophys. Res.*, *101*, 19,465–19,481, 1996.

Holben, B. N., et al., AERONET—A federated instrument network and data archive for aerosol characterization, *Remote Sens. Environ.*, *66*, 1–16, 1998.

Holben, B. N., et al., An emerging ground-based aerosol climatology: Aerosol optical depth from AERONET, *J. Geophys. Res.*, *106*, 12,067–12,097, 2001.

Kasten, F., and M. T. Young, Revised optical air mass tables and approximation formula, *Appl. Opt.*, *28*, 4735–4738, 1989.

Kaufman, Y. J., A. Gitelson, A. Karnieli, E. Ganor, R. S. Fraser, T. Nakajima, S. Mattoo, and B. N. Holben, Size distribution and scattering phase function of aerosol particles retrieved from sky brightness measurements, *J. Geophys. Res.*, *99*, 10,341–10,356, 1994.

Martínez-Lozano, J. A., M. P. Utrillas, F. Tena, R. Pedrós, J. Cañada, J. V. Boscá, and J. Lorente, Aerosol optical characteristics from summer campaign in an urban coastal Mediterranean Area, *IEEE Trans. Geosci. Remote Sens.*, *39*, 1573–1585, 2001.

Martínez-Lozano, J. A., R. Pedrós, C. Flamant, M. P. Utrillas, F. Tena, J. Moreno, J. Pelon, J. M. Cisneros, and C. González-Frias, A multi-instrument approach for characterizing the atmospheric aerosol optical thickness during the STAAARTE/DAISEX-99 campaign, *Geophys. Res. Lett.*, *29*(4), 1053, doi:10.1029/2001GL013585, 2002.

Martínez-Lozano, J. A., et al., Intercomparison of spectroradiometers for global and direct solar irradiance in the visible range, *J. Atmos. Oceanic Technol.*, *20*, 997–1010, 2003.

Moorthy, K. K., S. S. Babu, and S. K. Satheesh, Aerosol spectral optical depths over the Bay of Bengal: Role of transport, *Geophys. Res. Lett.*, *30*(5), 1249, doi:10.1029/2002GL016520, 2003.

Moreno, J., V. Caselles, J. A. Martínez-Lozano, J. Meliá, J. Sobrino, A. Calera, F. Montero, and J. M. Cisneros, The measurement programme at Barrax, in *DAISEX Final Results Workshop*, 43–52, ESA Publ. Div., ESTEC, Netherlands, 2001.

Nakajima, T., M. Tanaka, and T. Yamakuchi, Retrieval of the optical properties of aerosols from aureole extinction data, *Appl. Opt.*, *22*, 2951–2959, 1983.

Nakajima, T., G. Tonna, R. Rao, P. Boi, Y. Kaufman, and B. Holben, Use of sky brightness measurements from remote sensing of particulate polydispersions, *Appl. Opt.*, *35*, 2675–2686, 1996.

O'Dowd, C. D., and M. H. Smith, Physicochemical properties of aerosols over the northeast Atlantic: Evidence for wind speed related submicron sea salt aerosol production, *J. Geophys. Res.*, *98*, 1137–1149, 1993.

O'Neill, N. T., T. F. Eck, B. N. Holben, A. Smirnov, O. Dubovik, and A. Royer, Bimodal size distribution influences on the variation of Angstrom derivatives in spectral and optical depth space, *J. Geophys. Res.*, *106*, 9787–9806, 2001.

O'Neill, N. T., T. F. Eck, B. N. Holben, A. Smirnov, A. Royer, and Z. Li, Optical properties of boreal forest fire smoke derived from Sun photometry, *J. Geophys. Res.*, *107*(D11), 4125, doi:10.1029/2001JD000877, 2002.

Penner, J. E., L. Reaitch, D. Murphy, J. Nganga, and G. Pitari, The aerosols, their direct and indirect effects, in *Climate Change: The Scientific Basis*, edited by J. Hougthton et al., pp. 289–348, Cambridge Univ. Press, New York, 2001.

Ponchaut, F., Processing of the POLDER airborne data acquired during the DAISEX'99 campaign, Noveltis, *TR/7013/00/002*, 2000.

Remer, L. A., and Y. J. Kaufman, Dynamic aerosol model: Urban/industrial aerosol, *J. Geophys. Res.*, *103*, 13,859–13,871, 1998.

Remer, L. A., S. Gassó, D. A. Hegg, Y. J. Kaufman, and B. N. Holben, Urban/industrial aerosol: Ground-based sub/sky radiometer and in situ measurements, *J. Geophys. Res.*, *102*, 16,849–16,859, 1997.

Remer, L. A., Y. J. Kaufman, and B. N. Holben, Interannual variation of ambient aerosol characteristics on the coast of the United States, *J. Geophys. Res.*, *104*, 2223–2231, 1999.

Russell, P., et al., Pinatubo and pre-Pinatubo optical depth spectra: Mauna Loa measurements, comparisons inferred particle size distributions, radiative effects, and relationships to lidar data, *J. Geophys. Res.*, *98*, 22,969–22,985, 1993.

Sánchez-Muniosguren, L., E. Cuevas, and B. De la Morena (Eds.), *Results of First Iberian UV-VIS Instruments Intercomparison*, Min. de Medio Ambiente, Madrid, in press, 2003.

Schmid, B., C. Mätzler, A. Heimo, and N. Kämpfer, Retrieval of optical depth and particle size distribution of tropospheric and stratospheric aerosols by means of sun photometry, *IEEE Trans. Geosci. Remote Sens.*, *35*, 172–182, 1997.

Schwartz, S. E., and M. O. Andreae, Uncertainty in climate change caused by aerosols, *Science*, *272*, 1121–1122, 1996.

Shifrin, K. S., Simple relationships for the Angstrom parameter of disperse systems, *Appl. Opt.*, *34*, 4480–4485, 1995.

Smirnov, A., Y. Villevalde, N. T. O'Neill, A. Royer, and A. Tarussov, Aerosol optical depth over the ocean: Analysis in terms of synoptic air mass types, *J. Geophys. Res.*, *100*, 16,639–16,650, 1995.

Smirnov, A., B. N. Holben, O. Dubovik, N. T. O'Neill, L. A. Remer, T. F. Eck, I. Slutsker, and D. Savoie, Measurements of atmospheric optical parameters on U.S. Atlantic coast sites, ships, and Bermuda during TARFOX, *J. Geophys. Res.*, *105*, 9887–9901, 2000.

Smirnov, A., B. N. Holben, Y. J. Kaufman, O. Dubovik, T. F. Eck, I. Slutsker, C. Pietras, and R. N. Halthore, Optical properties of atmospheric aerosol in maritime environments, *J. Atmos. Sci.*, *59*, 501–523, 2002.

Smirnov, A., B. N. Holben, O. Dubovik, R. Frouin, T. F. Eck, and I. Slutsker, Maritime component in aerosol optical models derived from Aerosol Robotic Network data, *J. Geophys. Res.*, *108*(D1), 4033, doi:10.1029/2002JD002701, 2003.

Utrillas, M. P., Estudio de aerosoles a partir de medidas de irradiancia solar spectral (in Spanish), Ph.D. thesis, Valencia Univ., Spain, 1995.

Utrillas, M. P., R. Pedrós, J. A. Martínez-Lozano, and F. Tena, A new method for determining the Angstrom turbidity coefficient from broadband filter measurements, *J. Appl. Meteorol.*, *39*, 863–874, 2000.

Utrillas, M. P., R. Pedrós, J. L. Gómez, and J. A. Martínez-Lozano, Ground based measurements of spectral solar irradiance (global, direct and diffuse) and spectral sky radiance at Barrax (1998, 1999 and 2000), in *DAISEX Final Results Workshop*, pp. 63–70, ESA Publ. Div., ESTEC, Netherlands, 2001.

Vasilyev, O. B., et al., Spectroradiometer based on wedge interference filters (SWIF): Spectral optical depths at Mauna Loa observatory, *Appl. Opt.*, *34*, 4426–4436, 1995.

Volz, F., Photometer mit Selen-photoelement zur spaktralen Messung der Sonnestrahlung und zur Bestimmung der Wallenlangeabhangigkeit der Dunstrubung, *Arch. Meteorol. Geophys. Bioklimatol.*, *10*, 100–131, 1959.

J. L. Gómez-Amo, J. A. Martinez-Lozano, R. Pedrós, F. Tena, and M. P. Utrillas, Grupo de Radiación Solar, Departamento de Termodinámica, Universitat de Valencia, Dr. Moliner 50, 46100 Burjassot (Valencia), Spain. (Jose.A.Martinez@uv.es)